International Journal of Nanomedicine

Dovepress
Taylor & Francis Group

Open Access Full Text Article

ORIGINAL RESEARCH

ROS-Responsive Biomimetic Nanocomplexes of Liposomes and Macrophage-Derived Exosomes for Combination Breast Cancer Therapy

Minhao Xu[1,*], Lu Bai[1,*], Meng Sun[1], Xinlei Yan[1], Ying Xiong[2], Yu Wang[1], Yue Guo[1], Xingyou Liu[1], Leijie Yu[1], Xing Zhong[1], Mengqiong Ran[1], Ben Wang[3], Yaqin Tang[1], Robert J Lee[4], Jing Xie[1]

[1]School of Pharmacy and Bioengineering, Chongqing University of Technology, Chongqing, 400054, People's Republic of China; [2]Enrollment and Employment Department, Alumni-Office, Chongqing University of Technology, Chongqing, 400054, People's Republic of China; [3]Chengcheng County Hospital, Weinan, 715200, People's Republic of China; [4]College of Pharmacy, The Ohio State University, Columbus, OH, 43210-1291, USA

*These authors contributed equally to this work

Correspondence: Jing Xie, Chongqing University of Technology, 69 hongguang Road, Chongqing, 400054, People's Republic of China, Email xiejing33@cqut.edu.cn

Purpose: Breast cancer is the most diagnosed cancer in women globally and it poses a major threat to women's lives and health. As an essential therapeutic approach for breast cancer, chemotherapy encounters various clinical challenges like multidrug resistance and systemic toxicity. Nanotechnology has shown progress in addressing chemotherapy drug limitations. However, externally introduced nanoparticles are typically captured by the mononuclear phagocyte system (MPS) post-administration. To mitigate chemotherapy drug toxicity and enhance drug delivery efficiency, we combined ROS-responsive cationic liposomes (cLip) with macrophage-derived exosomes to create biomimetic nanocomplex (E-cLip-DTX/si) for co-delivery docetaxel (DTX) and Bcl-2 siRNA.

Methods: We encapsulated docetaxel (DTX) and Bcl-2 siRNA as model drugs into biomimetic nanocomplexes and validated their antitumor efficacy in vitro and in vivo.

Results: In vitro and vivo tests show that E-cLip-DTX/si can react to ROS, promote apoptosis of tumor cells effectively, and prolong circulation time. In breast cancer mouse model, E-cLip-DTX/si displays notable tumor accumulation efficiency, remarkable anti-tumor effects, and a favorable safety profile.

Conclusion: We have developed a ROS-responsive biomimetic nanocomplexes that efficiently delivers DTX and Bcl-2 siRNA into the tumor site, overcoming the MPS barrier and extending the blood circulation time of the drug. Hence, biomimetic nanocomplex is a promising drug delivery platform with controlled drug release and biocompatibility for effective anti-tumor treatment.

Keywords: co-delivery, RNAi, biomimetic delivery, combination therapy

Introduction

Breast cancer, as one of the most prevalent malignancies, presents a significant risk to the health of women.[1] Despite extensive global research efforts by scientists to combat this grave and lethal disease,[2,3] the worldwide incidence of breast cancer continues to rise steadily.[4] Presently, treatment for breast cancer comprises surgery, radiotherapy, chemotherapy,[5] targeted therapy,[6] and immunotherapy.[7–9] Chemotherapy, a primary clinical treatment method, can effectively eliminate tumor cells.[10] Currently, commonly used chemotherapeutic agents in clinical practice mainly include anthracyclines, paclitaxel, and certain antimetabolites,[11] which kill tumor cells and their proliferation by inducing DNA damage, blocking cell division, and interfering with DNA/RNA synthesis.[12] However, it also inevitably causes some level of damage to patients' normal cells due to its lack of specificity.[13] Furthermore, the frequent utilization of various chemotherapy drugs can lead to multidrug resistance (MDR),[14] complicating treatment further. Hence, there is a keen interest in enhancing chemotherapy by integrating it with other therapeutic approaches such as radiotherapy, immunotherapy, and RNAi.[15] Many clinical and preclinical studies have been conducted on these combined strategies to

Received: 26 December 2024
Accepted: 10 April 2025
Published: 24 April 2025

Graphical Abstract

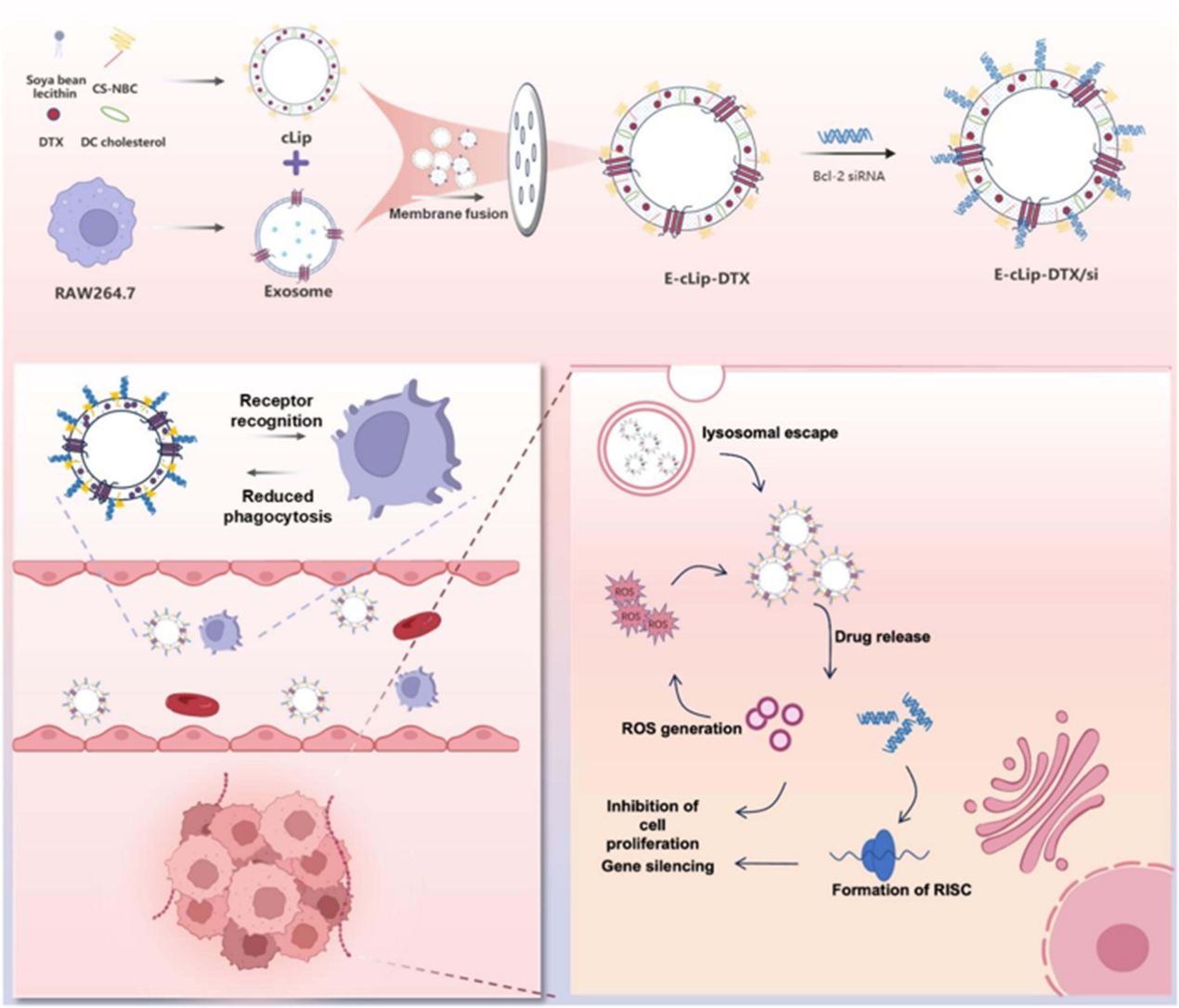

improve their effectiveness in suppressing tumors.[16] Nucleic acid drugs, with their specificity, high efficacy, and easy development, have emerged as promising options for treating tumors.[17,18] Nevertheless, the limited efficiency and instability of siRNA uptake,[19] as well as its susceptibility to degradation by nucleases and renal circulation metabolism,[20,21] hinder its widespread clinical application. Consequently, developing an efficient and stable delivery system to facilitate an effective combined treatment strategy represents a crucial barrier that needs to be overcome.

Exosomes (EVs) represent intrinsic nanoparticles secreted by cells, playing a pivotal role in intercellular communication, signaling, and the oversight of cellular functions.[22,23] They have surfaced as a promising drug carrier due to their low toxicity, remarkable biocompatibility, and outstanding ability to navigate physiological barriers.[24] Various scientific inquiries have underscored the effectiveness of exosomes as vehicles for drug conveyance to prolong drug presence in the system[24,25] and surmount physiological hindrances.[26,27] Nevertheless, a notable drawback persists in the limited capacity of exosomes to efficiently transport drugs.[26] Additionally, the modest exosome yield[28] and the complex surface functionalization process[29] alterations pose obstacles to the extensive use of exosomes as drug carriers.

As a widely utilized drug carrier, liposomes offer significant advantages in terms of multifunctionality, yield, drug loading efficiency, and standardization.[30,31] Dozens of FDA-approved liposomal drug delivery systems have been clinically validated and commercialized.[32] These minute lipid vesicles effectively transport drugs to tumor cell vicinity, thereby reducing adverse effects on normal cells. Notably, utilizing abnormal physiological signals (such as acidity, ROS concentration,[33] hypoxia,[34] specific enzyme expression[35]) in the tumor microenvironment (TME) for the optimized design of liposomes has become an important research direction.[36] However, challenges such as material toxicity and susceptibility to liver and spleen clearance persist.[37,38] Hybrid membrane nanovesicles and biomimetic nanovesicles have emerged as promising solutions to overcome these hurdles.[39–41] Studies have highlighted the potential of mixed nanovesicles combining EVs and liposomes for drug delivery through methods like extrusion or freeze-thaw, offering a versatile drug delivery platform combining the strengths of both components.

Inspired by this, we have developed a ROS-responsive biomimetic nanocomplex (E-cLip-DTX / si) that integrates macrophage-derived exosomes (RAW247.6-Exo) with ROS-responsive cationic liposomes (c-Lip). This nanocomplex is used for cancer treatment combining RNAi and chemotherapy. Initially, we synthesized a compound with ROS-responsive properties based on the phenylboronic acid group (ROS-responsive group), known as CS-NBC, and prepared ROS-responsive cationic liposomes (c-Lip) by combining CS-NBC with the cationic lipid DC-Chol. The first-line agent (DTX, for breast cancer chemotherapy) is encapsulated within these liposomes. Subsequently, through extrusion, we obtained the biomimetic nanocomplex E-cLip-DTX. Our experimental results indicate that biomimetic nanocomplexes carry information from macrophages while retaining the ROS-responsive and cationic properties of liposomes. The positive charge carried by the biomimetic nanocomplexes facilitated the loading of Bcl-2 siRNA, enabling a therapeutic approach that combines RNAi with chemotherapy. Remarkably, DTX induces heightened ROS levels in tumor cells, enhancing carrier ROS sensitivity for rapid drug release at the tumor site. Both In vitro and in vivo results indicate that E-cLip-DTX / si can respond to ROS, effectively triggering tumor cell apoptosis while prolonging circulation time. In breast cancer mouse model, E-cLip-DTX / si exhibited substantial tumor inhibition and remarkable anti-tumor efficacy, accompanied by a favorable safety profile. Thus, the biomimetic nanocomplex presents itself as a promising drug delivery platform capable of precise and controlled drug release for efficient anti-tumor therapy.

Materials and Methods

Materials

Chitosan and docetaxel were procured from Macklin Biochemical Technology (Shanghai, China). 4-hydroxymethyl-benzene acid alcohol ester and p-nitrophenyl chloroformate were obtained from Bidepharm (Shanghai, China). Soy lecithin and DC cholesterol were sourced from AVT Pharmaceutical Tech Co., Ltd. (Shanghai, China). Bcl-2 siRNA was acquired from Ribobio (Guangzhou, China). DMEM medium, TSG101 and CD63 antibodies were purchased from Thermo Fisher (Beijing, China). RPMI medium 1640 was obtained from BasalMedia (Shanghai, China). FBS was sourced from ExCell Bio (Suzhou, China). All other chemicals used were of analytical grade and employed without further purification.

Cell Line

Murine 4T1 breast cancer cells and RAW 264.7 cells (Mouse Mononuclear Macrophages Cells) were purchased from the American Type Culture Collection (ATCC, USA). 4T1 cells were cultured in 1640 medium supplemented with 10% FBS and 1% penicillin-streptomycin, while RAW264.7 cells were cultured in DMEM medium supplemented with 10% FBS. All cells were incubated at 37°C with 5% (v/v) CO_2 in a humidified environment.

Synthesis and Characterization of CS-NBC

Following the procedure described by Li et al[42] 4-hydroxymethyl-phenylboric acid alcohol ester (0.5 g, 2.1 mmol) was dissolved in 10 mL of CH_2Cl_2, then combined with p-nitrophenyl chloroformate (0.47 g, 2.3 mmol) and triethylamine (0.6 mL, 4.3 mmol). The mixture was left to react for 2 hours at 4°C. Subsequently, any remaining triethylamine and p-nitrophenyl chloroformate were eliminated using 1 mol/L HCl, followed by a rinse with $NaHCO_3$ to remove the HCl,

and then dried with Na_2SO_4. The crude product was purified by silica gel column chromatography (ethyl acetate/petroleum ether = 1:20) and dried using a rotary evaporator to yield a yellow solid identified as NBC. A solution of 5 mg/mL NBC was slowly added into a 6 mg/mL CS solution and stirred for 12 hours. The resulting light-yellow product obtained after freeze-drying was named CS-NBC. Confirmation of successful synthesis was achieved through Fourier transform infrared spectroscopy (FT-IR) and proton nuclear magnetic resonance spectroscopy (^{1}H NMR).

Preparation of ROS-Triggered Nanoparticles

Based on our previous work,[43] soybean lecithin and DC-cholesterol were dissolved in anhydrous ethanol as the oil phase at an 8:1 mass ratio. Simultaneously, CS-NBC was dissolved in DEPC water as the aqueous phase at a concentration of 0.5 mg/mL, and equal volumes of the above two solutions were passed through the microfluidic chip at a flow rate of 0.8 mL/min to prepare cationic liposomes, respectively. The lipid suspension was subsequently extruded through a 0.2 μm polycarbonate membrane filter 10 times to achieve a uniform cLip. The process for preparing drug-loaded liposomes mirrored that of cLip, with the addition of DTX exclusively to the oil phase.

Preparation of ROS-Triggered Biomimetic Nanocomplexes

Exosomes were isolated from the RAW264.7 cell supernatant through ultra-high-speed centrifugation. Initially, the cell supernatant was centrifuged at 300g at 4°C for 10 minutes to eliminate cell debris and impurities, followed by exosome retrieval through centrifugation at 110,000g for 70 minutes. Subsequently, for additional purification, the exosomes obtained previously underwent centrifugation using a purification column at 4000g at 4°C for 5 minutes. The cationic liposomes acquired earlier were combined with exosomes isolated from an equal-volume cell supernatant. According to the method described previously,[44] identical amounts of Exosome and cLip were sequentially extruded 10 times through 1.0, 0.4, and 0.2 μm polycarbonate membranes using a micro-extruder (Avanti Polar Lipids) to produce E-cLip. Finally, they were mixed with Bcl-2 siRNA and left to incubate for 20 minutes to yield E-cLip-si or E-cLip-DTX/si.

Physicochemical Examination

The liposomes, exosomes, and biomimetic nanocomplex's particle size and surface potential were gauged using a PALS particle size potentiometer (Brook, USA), and their structure was visualized via transmission electron microscopy (JEOL, Japan). In brief, Exosome, cLip, and E-cLip were diluted and applied to a copper grid. Post air drying, they were observed under a transmission electron microscope at 100kV. Encapsulation efficiency (EE) was evaluated by HPLC through measuring the encapsulation concentration and total drug concentration. A C18 reversed-phase chromatography column with a mobile phase ratio of acetonitrile to water at 65:35 was used, with DTX content being identified after adding methanol as a demulsified. EE (%) calculation: EE (%) = WE/WT * 100%, where WE represent the weight of DTX encapsulated in the nanocomplex, and WT denotes the total DTX weight in the preparation. The longevity of the biomimetic nanocomplex was studied by monitoring changes in particle size, PDI, and potential over a 14-day period, the adsorption efficiency of siRNA by biomimetic nanocomplex was assessed using gel electrophoresis.

Protein Analysis of Exosomes, cLip, and E-cLip

The protein content in exosomes was measured using the BCA assay kit (Biosharp, Anhui). Western blot analysis was conducted to identify the expression of characteristic proteins TSG101 and CD63 in exosomes. SDS-PAGE was utilized to analyze the overall protein profiles of Raw264.7 cells, Exosome, cLip, and E-cLip.

Verification of E-cLip Fusion

To confirm the successful fusion of Exosome and cLip, exosomes were stained with Dil fluorescent dye (Beyotime, Nanjing), and liposomes were labeled with fluorescein isothiocyanate FITC (Energy Chemical, Shanghai) using confocal laser microscopy (CLSM, Carl Zeiss, Shanghai, Germany) for observation of the membrane fusion.

Fluorescent Resonance Energy Transfer (FRET) was also employed for further validation of membrane fusion. FITC (Energy Chemical, Shanghai) and Rhodamine B (Macklin, Shanghai) were added in equal molar ratio to the oil phase to create double-fluorescently labeled liposomes. FITC (excitation/emission = 490/520 nm) served as the electron donor,

while Rhodamine B (excitation/emission = 536/568 nm) served as the electron acceptor. The emission spectra of liposomes pre and post membrane fusion were recorded in the range of 500–700 nm with an excitation wavelength of 470 nm.

Validation of ROS-Triggered Biomimetic Nanocomplexes

Pyrocinol functional groups in ARS can react with phenyl boric acid groups to produce fluorescent polymers. ARS was utilized to confirm the ROS sensitivity of nanoparticles. Specimens with various functional groups were exposed to 0.005% ARS solution (Solarbio, Beijing) for 1 hour. Subsequently, the emission spectrum ranging from 500–700nm under excitation at 490 nm was assessed using a multifunctional enzyme marker, and fluorescence intensity at 620nm was analyzed to plot a curve. Subsequently, the particle size changes of nanocomposites were investigated under an H_2O_2 environment using PALS. In brief, cLip and E-cLip were incubated with a 5 mm H_2O_2 solution at 37°C for 2 hours, followed by PALS analysis to assess their environmental responsiveness.

The environmentally triggered release behavior of E-cLip-DTX was evaluated through HPLC. E-cLip-DTX was dissolved in a sealed bag containing 5mM H_2O_2 solution (MWC0=4000) with a control setup. The sealed bags were immersed in a release medium comprising 40 mL Tween 80, and the system was agitated at 80 rpm/min on a shaking table at 37°C. Samples were withdrawn at specified intervals while simultaneously replenishing an equal volume of fresh release medium, and their DTX content was analyzed by HPLC (Shimadzu, Japan) to generate a curve.

Intracellular ROS Detection

The ROS generated by 4T1 cells treated with various compounds was visualized using CLSM. 2×10^5 4T1 cells were seeded in confocal culture plates and incubated for 24 hours. Following a 6-hour stimulation with the compounds, any remaining compounds were washed off with PBS. Subsequently, ROS fluorescence was assessed using the DCFH-DA probe (Beyotime, Nanjing). Fluorescence images were captured using CLSM. ROS fluorescence intensity was quantified using flow cytometry, similar to the previous procedure, after the DCFH-DA probe staining was completed, the cells were digested down using trypsin, resuspended in PBS and then the fluorescence intensity was detected at 488 nm by flow cytometry (BD FACSCelesta, USA).

Biomimetic Nanocomplex Escape Macrophage Uptake and Blood Circulation Assays

The internalization of biomimetic nanocomplexes containing RBITC by RAW264.7 cells was visualized using CLSM. 2×10^5 RAW264.7 cells were seeded in confocal culture plates and incubated in a 5% CO_2 environment at 37°C for 24 hours. Subsequently, cLip-RBITC and E-cLip-RBITC were introduced. The concentration of RBITC was maintained at 0.05 μg/mL. Following a 4hour treatment period, the dye was rinsed with PBS, fixed with 4% paraformaldehyde (Biosharp, Anhui), and nuclei were stained with DAPI staining solution (Beyotime, Nanjing) for 10 minutes. CLSM scanning was then conducted. The fluorescence intensity of cellular uptake was quantitatively assessed using flow cytometry.

Balb/C breast cancer mice (n=3) that had been successfully engrafted with 4T1 cells were intravenously injected with biomimetic nanocomplexes coated with DiR dye (0.5mg/kg, Macklin, Shanghai). Subsequently, blood samples were collected from the tail tips of the mice at specific time intervals and analyzed using the Alliance Q9 chemiluminescence imaging system (UVITEC, Shanghai, UK) to capture fluorescent images of the blood.

Cellular Uptake and Lysosomal Escape

Using confocal laser scanning microscopy (CLSM), observe the internalization of biomimetic nanocomplexes in 4T1 cells. 2×10^5 4T1 cells were seeded in confocal culture plates and incubated in a 5% CO_2 environment at 37°C for 24 hours. Subsequently, fluorophore-containing drugs were added. RBITC was used at a concentration of 0.05 μg/mL along with FAM-siRNA (50 nM, Sangon Biotech, Shanghai). After 4 hours of incubation, the dye was removed with PBS, fixed with 4% paraformaldehyde (Biosharp, Anhui), and stained with DAPI (Beyotime, Nanjing) for 10 minutes to label the nucleus. CLSM imaging was then performed. Flow cytometry was utilized for quantifying the fluorescence intensity of various formulations.

Similar experimental procedures were followed for assessing cellular uptake. Following treatment of 4T1 cells at 37°C for 1, 2, and 4 hours with different preparations, the fluorescent dye was washed away using PBS. Lysosomes were labeled with LysoTracker™ Red (1:10000, ThermoFisher, Beijing), washed with PBS three times, fixed with 4% paraformaldehyde, stained with DAPI to label the nuclei. Ultimately, lysosomal escape was visualized and imaged using confocal laser scanning microscopy.

Cell Viability

The safety of biomimetic nanocomplexes was confirmed through CCK-8 experiments, assessing the toxicity of nanocarriers before and after membrane fusion on 4T1 and RAW264.7 cells. In brief, 1×10^4 4T1 and RAW264.7 cells were seeded separately into 96-well plates and allowed to grow for 24 hours. After reaching the logarithmic phase, cells were treated with cLip and E-cLip for another 24 hours. Subsequently, 100 μL of 10% Cell Counting Kit-8 (CCK-8, Biosharp, Anhui) was added and incubated for 4 hours. The absorbance at a wavelength of 450 nm was then measured using a multifunctional enzyme marker.

To determine the optimal combination ratio of DTX and Bcl-2 siRNA for the most effective anti-tumor outcome, 4T1 cells (1×10^4 cells/well in a 96-well plate) were treated with E-cLip-DTX/si according to the protocol established by Chen's group.[45] Various DTX: Bcl-2 siRNA ratios of 3:1, 2:1, 1:1, 1:2, and 1:3 was diluted in DMEM medium and added to the 4T1 cells for a 24-hour incubation. After the incubation period, the medium was replaced with 10% CCK-8 reagent and incubated for an additional 4 hours. The absorbance at 450 nm was then measured using an enzyme-labeler, and the relative cell viability was calculated relative to a negative control (PBS-treated cells).

Subsequently, we investigated the in vitro antitumor activity of E-cLip-DTX / si using the CCK-8 assay. We used a series of concentration gradients of Free DTX, E-cLip-DTX, E-cLip-si, E-cLip-DTX/si, to treat 4T1 cells and calculate their cell viability. In addition, we calculated the combination index (CI) of the drugs using Compusyn software to assess the synergistic effect of DTX and Bcl-2 siRNA.

Evaluation of Cell Cycle Arrest and Apoptosis

5×10^4 4T1 cells were seeded into 24-well plates and incubated in a 5% CO2 atmosphere at 37°C for 24 hours. The cells were then exposed to various treatments for an additional 24 hours, with Docetaxel (DTX) at a concentration of 16 μg/mL and Bcl-2 siRNA at 10 nM. Following removal of the cell culture medium, enzymatic digestion was carried out, and the cells were pelleted by centrifugation in PBS at 1000 rpm for 5 minutes. Subsequently, cells were fixed in 70% ethanol for 24 hours, then centrifuged at 1000g for 5 minutes, washed thrice with PBS, and stained with propidium iodide (PI) staining solution (Regan Biology, Beijing) for 30 minutes. Finally, flow cytometry was used to measure the fluorescence intensity at a wavelength of 488 nm.

Apoptosis in cells subjected to different treatments was assessed using flow cytometry. Experimental procedures involved seeding and culturing 4T1 cells as described above, followed by drug stimulation. Adjust the docetaxel (DTX) concentration to 32 μg/mL and the Bcl-2 siRNA concentration at 20 nM. After removing the culture medium, cells were enzymatically dissociated without EDTA, pelleted at 4°C and 1000g in PBS for 5 minutes, repeated for a total of three washes. Cells were resuspended in 0.5 mL Binding Buffer and stained with 5 μL Annexin V-FITC and propidium iodide (PI) (Biosharp, Anhui) for 15–20 minutes. Apoptosis was then analyzed using flow cytometry.

Western Blot

To evaluate the In vitro silencing effectiveness of biomimetic nanocomplexes, 2×10^5 4T1 cells were seeded in 6-well plates for 24 hours. Subsequently, they were exposed to PBS, Free siRNA, Negative Control-siRNA (NC-siRNA), E-cLip-si, and E-cLip-DTX/si individually for another 24 hours. A mixture of 150 μL of protein lysate RIPA and PMSF (100:1, Solarbio, Beijing) was added and incubated on ice for 1 hour. The cells were then harvested using a cell scraper, and the resulting supernatant was centrifuged at 4 °C, 12000 g, for 10 minutes. A sample of the supernatant was used to determine the BCA protein content, while the rest was treated with protein loading buffer, followed by SDS-PAGE electrophoresis after denaturation at high temperature. The gel from the electrophoresis was transferred to a membrane,

blocked with 5% BSA, and incubated with the primary antibody overnight. After three washes, the membrane was incubated with the secondary antibody for 1 hour, washed again thrice, and finally used for protein visualization.

Breast Cancer Induction in BALB/c Mice

Transfer female Balb/C mice aged five weeks from Byrness Weil Biotech Ltd. (Chongqing, China) to six weeks of age by implementing adaptive feeding. Establish an in-situ tumor model by subcutaneously injecting 3×10^5 4T1 cells into the mammary pad on the right side of each mouse. All animal procedures were carried out following the ethical standards of the Animal Ethics Committee at Chongqing University of Technology.

Biodistribution and in vivo Antitumor Therapy

Injecting different preparations into BALB/C breast cancer model mice via tail vein, anesthesia the mice at 2,4,8,12, and 24 hours post-dosing and observing the fluorescence intensity of major organs in a small animal live imaging system.

In the evaluation of therapeutic efficacy in the in a mouse model of breast cancer, when the tumor size reaches 50–100mm3, the mice were randomly allocated into 7 groups (n=5) and administered a dose of 3mg/kg of DTX and 0.8mg/kg of Bcl-2 siRNA through intravenous injection every 3 days using PBS, DTX, Bcl-2 siRNA, E-cLip-DTX, E-cLip-si, cLip-DTX/si, E-cLip-DTX/si. Mouse body weight and tumor size were measured every 3 days. At the end of the experiment, mice were euthanized, major organs were collected, tumors were excised, photographed, and weighed. The formula for calculating tumor volume is as follows: Tumor volume (mm3) = (length) × $(\text{width})^2/2$.

Histopathological Examination

After euthanizing the mice, the heart, liver, spleen, lungs, kidneys, and tumor were fixed in 4% paraformaldehyde, dehydrated using a gradient, embedded in paraffin, sectioned, dewaxed, stained with hematoxylin and eosin, dehydrated, and observed under a fluorescence microscope (Zeiss, Germany).

TUNEL Assay and Immunohistochemistry

TUNEL Detection: Following 30 minutes of incubation in 0.1% Triton X-100, sections were washed with PBS and subjected to TUNEL detection using the instructions provided by the TUNEL detection kit (Biosharp, Anhui). After DAPI staining, sections were observed under a microscope.

Ki-67, Bcl-2 immunohistochemistry: Immunohistochemistry was conducted to assess the expression of Ki-67 and Bcl-2 in tumor cells of each mouse group. Tumor sections were paraffin-treated, rehydrated, subjected to antigen retrieval, incubated with Ki-67 and Bcl-2 antibodies (Cell Signalling, USA) overnight, and secondary antibodies (Thermo Fisher, Beijing) were added before microscopic examination.

Statistical Analysis

All data are presented as mean ± standard deviation. One-way analysis of variance (ANOVA) was used to analyze the difference between the control and experimental groups. Statistical significance was set to $p < 0.05$, and the p-value was expressed by asterisk as follows: * $p < 0.05$, ** $p < 0.01$, *** $p < 0.001$, **** $p < 0.0001$; NS, no significance.

Results

Synthesis and Characterization of ROS-Responsive Materials

The synthetic route of the ROS-sensitive CS-NBC material and the H-NMR identification map are shown in Figures S1 and S2. The characteristic peak of p-nitro group appeared at δ=7.74ppm, and the proton peak at δ =7.39ppm and δ =7.78ppm; δ = 3.6–4.0ppm signal refers to the characteristic peak of CS, confirming the successful connection between CS and NBC. FT-IR was utilized to demonstrate the synthesis of CS-NBC. The FT-IR spectra of the CS, NBC, and CS-NBC are shown in Figure S3. The characteristic peak at 2874 cm-1 is the expansion vibration peak of chitosan methyl at 1588 cm-1,1157 cm-1 is the bending vibration peak of the primary alcohol in chitosan, the 1081 cm-1 peak in NBC, and 823 cm-1 expansion vibration peak proves the introduction of a benzene ring at 1115 cm-1 and 1588 cm-1, confirming the successful synthesis of CS-NBC.

Preparation and Characterization of the Biomimetic Nanocomplexes

To evade clearance of nanoparticles by the MPS and prolong the circulation duration of medications, we developed the ROS responsive biomimetic nanocomplexes E-cLip-DTX/si (Scheme1). Exosomes were isolated from the medium supernatants of mouse monocyte macrophage RAW264.7 via ultracentrifugation, and Western blot analysis verified the existence of the characteristic protein (Figure 1C). The exosome particles measured between 70 and 95 nm in size (Figure 1A) with a surface potential of approximately −9 mV (Figure 1B). After negative staining with phosphotungstic acid, TEM images showed that spherical vesicles were successfully extracted (Figure 1D). Cationic liposomes were produced using microfluidic technology, resulting in uniform particle sizes and enhanced stability compared to other methods. Analysis by transmission electron microscopy and Dynamic Light Scattering (DLS) revealed that the spherical liposomes ranged from 55 to 80 nm in size (Figure 1A), with a surface potential of around 36 mV (Figure 1B).

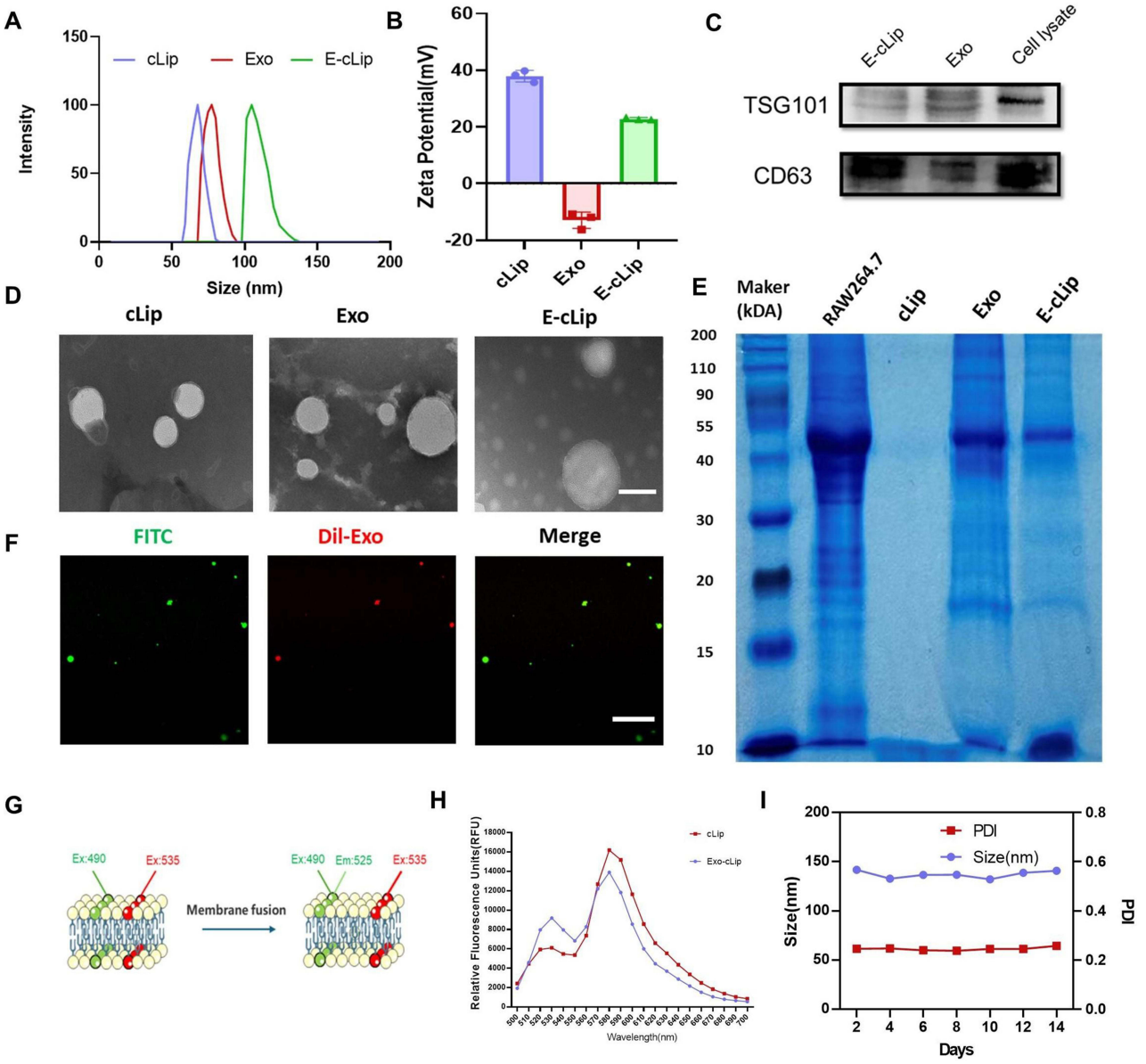

Figure 1 Preparation and characterization of biomimetic nanocomplexes. (**A**) Size distribution of DLS for cLip/Exo/E-cLip. (**B**) Magnitude of Zeta potential for cLip/Exo/E-cLip. (**C**) Protein imprint analysis of TSG101 and CD63 in Exo, E-cLip, and RAW264.7 cell lysate. (**D**) TEM images of cLip/Exo/E-cLip. Scale bar: 100 nm (**E**) SDS-PAGE images of RAW264.7 cell lysate, cLip, Exo, and E-cLip. (**F**) Fluorescence colocalization images of cLip and Exo membranes post-fusion using CLSM. (**G**) Schematic diagram showing changes in emitted fluorescence intensity of FITC and RBITC pre and post fusion. (**H**) Fluorescence spectra of cLip and E-cLip pre and post fusion. (**I**) Measurement of size and PDI of E-cLip for 14 days.

Subsequently, we constructed biomimetic nanocomplexes by successive extrusion of liposomes and exosomes through a 200 nm polycarbonate membrane. This process led to a slight increase in particle size, with hybrid particles measuring approximately 110 nm (Figure 1A) and a surface potential of 24 mV (Figure 1B). The increased particle size and altered surface potential indicates the successful transfer of the membrane onto ROS-responsive nanoparticles. Characterization under transmission electron microscopy showed that the E-cLip structure appeared uniformly rounded with a nuclear-shell-like morphology (Figure 1D).

To confirm the successful merging of biomimetic nanocomplexes, exosomes and liposomes were tagged with RBITC and DiL, respectively. The co-localization of exosomes and liposomes was visually observed using CLSM (Figure 1F). Subsequently, the fluorescence resonance energy transfer (FRET) provided further confirmation of the successful fusion between the exosome and liposomes (Figure 1G). As shown in the schematic diagram (Figure 1G), we prepared fluorescently labeled liposomes with equimolar ratios of FITC and rhodamine B. The results showed that FITC and rhodamine B were used for the fusion of exosomes and liposomes. Since the emission wavelength of FITC overlapped with the excitation wavelength of rhodamine B, part of the emission light of FITC was used to excite rhodamine B (Figure 1H). And after membrane fusion, we found that the emission peak of FITC at λem=530 nm was elevated, while that of rhodamine B at λem=580 nm was decreased (Figure 1H), which indicated that the insertion of EV content in the lipid bilayer of liposomes led to a larger distance between the two fluorescent dyes. The above results verify the successful fusion of exosome and liposome membranes.

In addition, we analyzed the protein profiles of RAW264.7 cells, Exo, cLip, and E-cLip through SDS-PAGE experiments (Figure 1E). The bionic nanocomplexes exhibited a protein distribution similar to that of the Exosome and different from that of the RAW264.7 cells, which implies that they inherited the surface receptors and membrane proteins of the Exosome. Regarding drug loading efficiency, HPLC was utilized to quantify the DTX content in cLip-DTX and E-cLip-DTX, the encapsulation efficiency values were calculated based on the standard curves (Figure S4) to be 96.5 ± 2.60% and 91.1 ± 1.34%, respectively. The binding capacity of the nanocomplexes to siRNA was evaluated through agarose gel electrophoresis experiments. Analysis in Figure S5 revealed the band of siRNA completely disappears when the N/P ratio of 8, indicating the cations in the nanocomplexes can completely adsorb siRNA. E-cLip displayed a similar siRNA absorption efficiency to cLip, hence an N/P ratio of 8 was adopted as their binding ratio for subsequent studies. Subsequent examination focused on the size changes of E-cLip over a 14-day period to assess its stability, demonstrating a constant particle size of 120–140 nm, PDI range of 0.2–0.3 (Figure 1I), and a zeta potential of 24 mV (Figures S6), affirming the stability of E-cLip.

Sensitivity Investigation of ROS in Nanocomplexes and Induced ROS Generation

The catechol group in ARS produces a fluorescent polymer when reacting with the phenylboronic acid group, by which we can verify the ROS responsiveness of the nanocomplexes by the change in fluorescence intensity. As illustrated in Figures S7 and 2A, the emission intensity of cLip + ARS or E-cLip + ARS was higher compared to cLip, E-cLip, or ARS alone. However, the presence of H_2O_2 hindered this emission enhancement, suggesting that the phenylboronic acid group in cLip or E-cLip has been degraded under H_2O_2 conditions. The alteration in particle size of cLip or E-cLip in the presence of H_2O_2 was monitored using DLS. Figure 2B demonstrates that following exposure to H_2O_2 for 1 hour, the particles lost their uniformity and stability. Subsequent investigation focused on the ROS-responsive release of biomimetic nanocomplexes coated with DTX. Calculation of drug release at different time points from standard curves, as depicted in Figure 2C, the elevated ROS environment induced by H_2O_2 led to an accelerated release of DTX, with the cumulative release rate reaching 65% after 24 hours. It was shown that the biomimetic nanocomplexes were sensitive to the ROS environment and could achieve rapid drug release in the presence of ROS.

It has been reported that DTX can elevate the level of ROS within tumor cells.[46] This characteristic enables us to enhance the controlled release of biomimetic nanocomplexes at the tumor sites. 4T1 cells were exposed to varying concentrations of DTX, and ROS generation in the tumor cells was observed 6 hours later using the DCFH-DA probe. DCFH-DA itself is non-fluorescent but is converted to DCFH by esterase upon entry. DCFH is then oxidized by ROS to form fluorescent DCF, with the green fluorescence indicating the level of intracellular ROS generation. In Figure 2D–E, it can be seen that the control group exhibited minimal fluorescence, whereas DTX led to increased DCF green

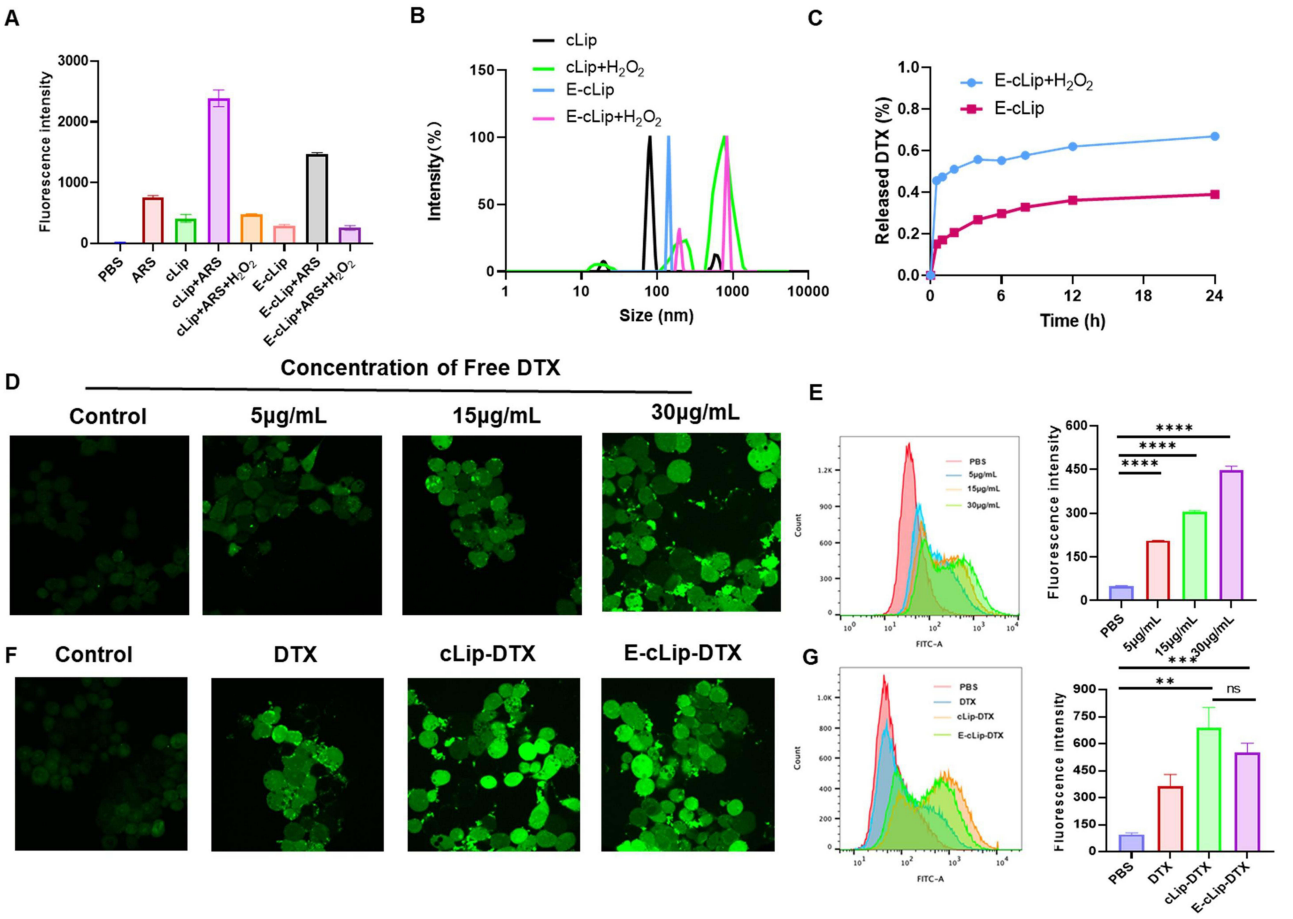

Figure 2 In vitro ROS responsiveness of biomimetic nanocomplexes and DTX promotion of ROS generation in 4T1 cells. (**A**) Fluorescence intensity of ARS at 620 nm wavelength under different conditions. (**B**) Size distribution of cLip and E-cLip in the presence or absence of H_2O_2. (**C**) Release efficiency of E-cLip-DTX with or without H_2O_2. (**D**) DCF staining of 4T1 cells treated with different concentrations of DTX (5 μg/mL, 15 μg/mL, 30 μg/mL) and (**F**) under different formulations (C_{DTX}=15 μg/mL) observed using CLSM. Scale bar:40 μm. (**E**) Flow cytometry and histogram reflecting ROS generation in 4T1 cells treated with different concentrations of DTX (5 μg/mL, 15 μg/mL, 30 μg/mL) and (**G**) under different formulations (C_{DTX}=15 μg/mL). Data presented as mean ± standard deviation (n = 3, ****p < 0.0001, **p < 0.01, ns, not significant).

fluorescence and a dose-dependent rise in ROS production by DTX. Further investigation into the impact of different DTX-loaded preparations on ROS production in 4T1 cells was conducted. As illustrated in Figure 2F and G, cells treated with DTX, cLip-DTX, and E-cLip-DTX displayed significantly stronger fluorescence compared to controls, with fluorescence intensity quantified using flow cytometry. These findings suggest that our biomimetic nanocomplexes can achieve precise ROS-controlled drug release. In addition, the released DTX can further promote the production of ROS by tumor cells, thus facilitating a more rapid and efficient release of chemotherapeutic and nucleic acid drugs.

Biomimetic Nanocomplexes Have the Capability to Significantly Extend the Duration of Blood Circulation

To determine whether the membrane-fused biomimetic nanocomplexes could resist the clearance of MPS, RAW 264.7 was used to simulate the In vitro clearance of MPS, referring to the method of Liu et al,[47] we incubated various nanoparticles with RAW264.7 cells and observed nanoparticle phagocytosis using confocal microscopy. We found that the red fluorescence around the nucleus of RAW264.7 cells in the cLip group was very pronounced, whereas the red fluorescence of E-cLip-treated RAW264.7 cells was minimal (Figure 3A). Flow cytometry quantification of fluorescence uptake by RAW264.7 cells was consistent with the confocal laser scanning microscopy (CLSM) results (Figure 3B), indicating reduced nanoparticle uptake by macrophages following exosome membrane fusion. This may be due to the

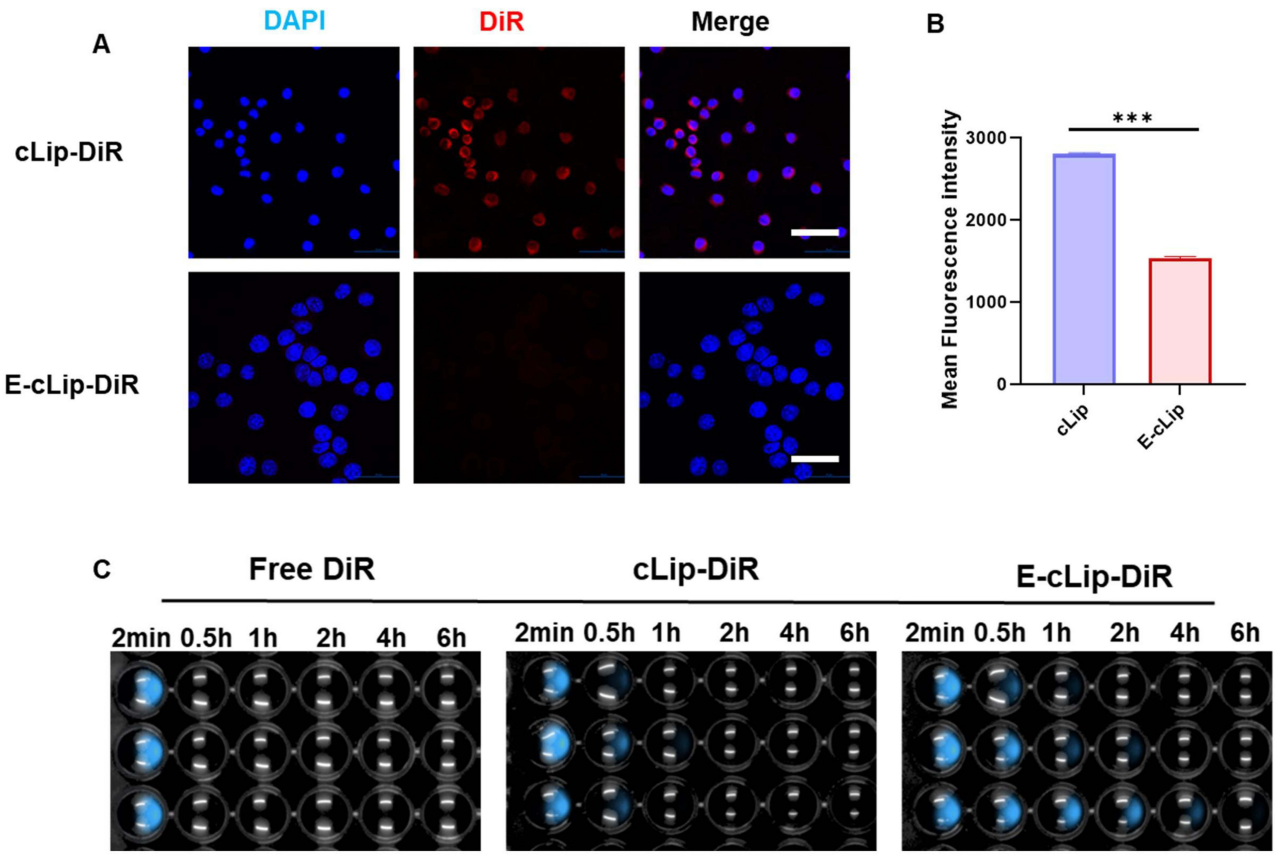

Figure 3 Biomimetic nanocomplexes (E-cLip-DiR) carrying macrophage information reduces macrophage endocytosis and improves blood circulation. (**A**) Images of cLip-DiR and E-cLip-DiR uptake taken in RAW264.7 cells by CLSM. Scale bar:40 μm. (**B**) Flow cytometry was used for quantitative analysis of the uptake of different nanocarriers by RAW264.7 cells (n=3). (**C**) Blood clearance (n=3) of DIR-labeled different nanoparticles in Balb/C mice, at each time interval, blood samples were collected from the tail and placed in a 96-well blackboard and imaged by the Alliance Q9 chemiluminescence imaging system. Data are expressed as the mean ± SD (n = 3, ***p < 0.001).

integration of homologous membrane proteins from macrophage-derived exosome membranes onto the surface of the nanocomplexes after membrane fusion, thereby reducing phagocytosis by macrophages. In addition, the experimental results of CCK8 corroborated this view, and we compared E-cLip-DTX and free DTX with RAW264.7 cells for 24 h, respectively, and the results showed that E-cLip-DTX was almost non-toxic to RAW264.7 cells in comparison to DTX (Figure S8). This indicates that RAW264.7 cells did not take up E-cLip-DTX, proving that the bionic nanocomplexes were effective in reducing phagocytosis by macrophages. To assess the blood circulation time of the different preparations, free DiR, cLip-DiR, and E-cLip-DiR were injected into mice via the tail vein. Mouse tail vein blood was collected at specified time points after injection for fluorescence signal detection. As depicted in Figure 3C, a minimal amount of fluorescence signal was detected in the cLip group after 1hour post-injection, while the E-cLip group exhibited sustained presence even after 2–4 hours post-injection, indicating favorable blood retention of E-cLip. The experimental findings demonstrate that E-cLip effectively evades DTX capture by the mononuclear phagocyte system to prolong drug circulation time in the bloodstream.

E-cLip-DTX / Si Cell Uptake Efficiency and Lysosomal Escape

RBITC, FAM-siRNA was used to mark nanocarriers, CLSM was utilized to see internalization of the cells following treatment with various preparations, and fluorescence was measured using flow cytometry in order to investigate the cellular internalization efficiency of E-cLip-DTX / si. Based on the CLSM results, we discovered that both liposomes and biomimetic nanocomplexes exhibit excellent cellular internalization efficiency, and whether they are loaded with siRNA has no effect on the uptake of the vector. Furthermore, compared to free siRNA, liposomes and biomimetic nanocomplexes displayed noticeably higher green fluorescence surrounding the nucleus (Figure 4A), indicating that our vector is

https://doi.org/10.2147/IJN.S514375

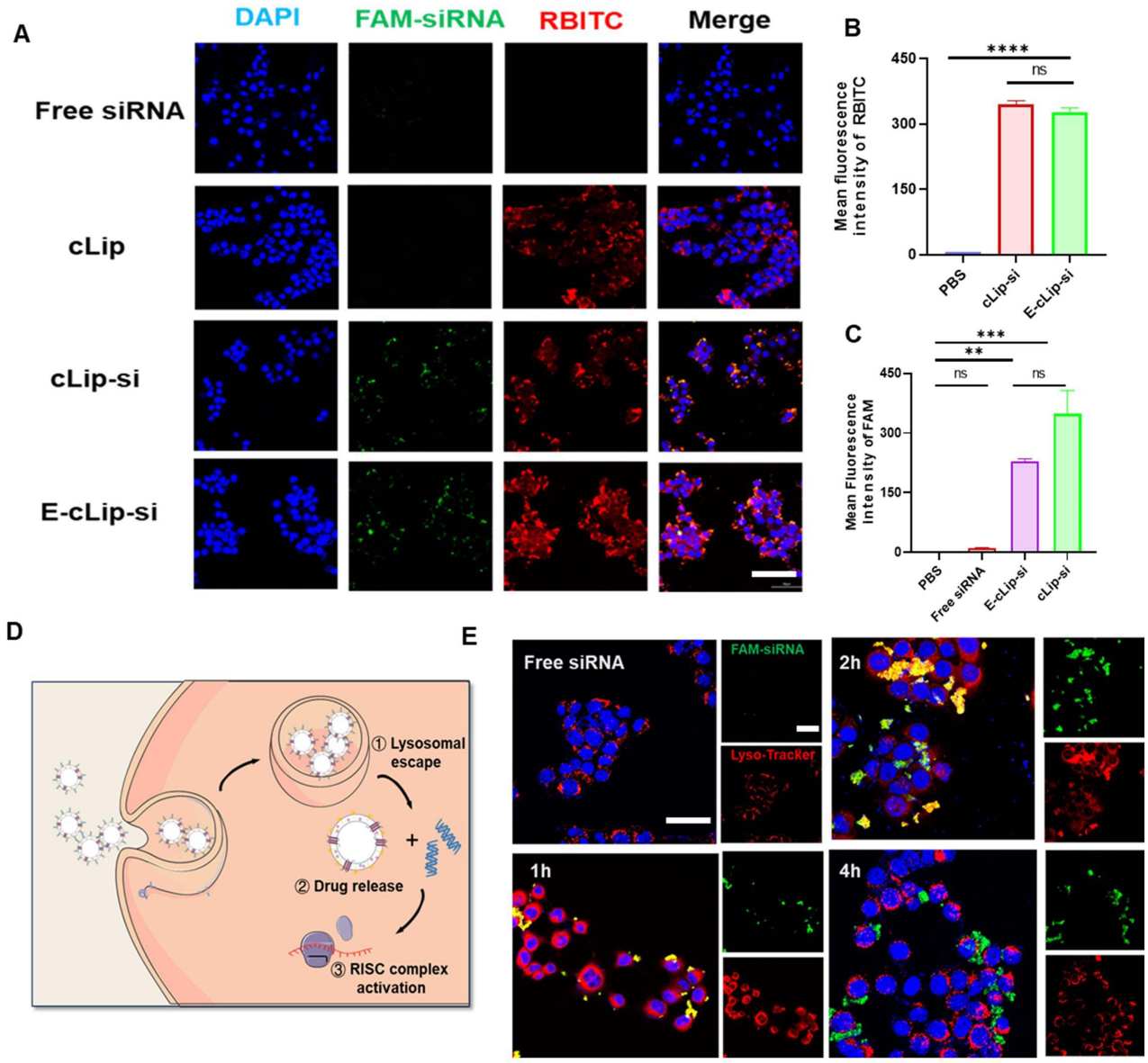

Figure 4 Cellular uptake and lysosomal escape of biomimetic nanocomplexes. (**A**) Cellular uptake of 4T1 cells with different formulations visualized by CLSM and (**B** and **C**) flow cytometry quantification of different formulations uptake. Scale bar:60 μm. (**D**) Schematic diagram of E-cLip-si entering the cell to achieve lysosomal escape and release the drug. (**E**) Images captured by CLSM showing the escape of E-cLip-si from cellular lysosomes in 1,2,4 hours. Scale bar:40 μm. Data presented as mean ± standard deviation (n = 3, ****p < 0.0001, ***p < 0.001, **p < 0.01, ns, not significant).

capable of effectively loading siRNA and internalizing into cells. Flow cytometry also demonstrated similar results to CLSM, further validating our conclusions. (Figure 4B and C). As shown in Figure 4D, one of the most important steps of utility is the successful escape of siRNA from lysosomes into the cytosol after entering the cell. Using CLSM, we ascertained the lysosomal escape of siRNA at 1, 2, and 4 hours (Figures S9 and 4E). The experimental results showed that free siRNA was difficult to escape capture and was rapidly degraded, while E-clip-si always maintained strong siRNA fluorescence. Additionally, the green fluorescence of FAM-siRNA gradually separated from the red fluorescence of the lysosome with the prolongation of time, suggesting that E-clip can effectively protect siRNA to accomplish lysosomal escape and carry out its gene silencing function.

In vitro Antitumor Effect of E-cLip-DTX / Si

We examined the harmful effects of several carriers (with or without membrane fusion) on RAW264.7 and 4T1 to confirm the safety of the vector. According to the experimental findings (Figure S10), cationic liposomes without membrane fusion exhibited significant cytotoxicity, which is in line with the earlier research. After membrane fusion, E-cLip had almost no effect on the cell viability of RAW264.7 cells and 4T1 cells, which proved the safety of the bionic nanocarriers. We then investigated E-cLip-DTX/si anti-tumor activity In vitro using CCK-8. We experimented with various ratios of DTX and Bcl-2 siRNA on 4T1 cells to find the ideal application ratio. The findings of the experiment demonstrated that the best outcomes were obtained with no discernible difference when the ratio of DTX to Bcl-2 siRNA was 2:1 or 3:1 (Figure 5A). Consequently, we decided to use the ratio of 2:1 in the next cytotoxicity tests. Next, we treated 4T1 cells with different preparations, and the results (Figure 5B) showed that the E-cLip preparation had a stronger tumor inhibitory effect compared to the free DTX group. This could be because the nanocarrier enhanced the cellular internalization efficiency of DTX. Furthermore, the group that was co-loaded exhibited the most robust anti-tumor activity. Although the cLip-DTX / si group exhibited the greatest tumor suppressive effect; however, this was due to the carrier's toxicity. Subsequently, to investigate whether DTX and BCL-2 siRNA had synergistic therapeutic effects at this ratio, we used the Compusyn software to calculate the drug's combination index (CI), which demonstrated that at this ratio, the CI value was less than one (Figure S11), indicating that DTX and Bcl-2 siRNA have a synergistic therapeutic effect. The above results indicate that the biomimetic nanocomplexes can co-deliver DTX and Bcl-2 siRNA into the cells and exerting their combined anti-tumor efficacy, while providing good safety.

Subsequently, we examined the cell cycle profile of the different agents after their action on 4T1 cells using flow cytometry (Figure 5D). Like previous reports,[48] DTX exhibited G2/M phase blockades without significant effect of siRNA, and the bionic nanocomplex E-cLip-DTX/si loaded with DTX showed the same results (Figure 5E). This suggests that biomimetic nanocomplexes can inhibit tumor cell proliferation by altering the cell cycle. We next examined apoptosis by flow cytometry after the action of different agents on 4T1 cells, as shown in Figure 5C. Untreated control cells showed a relatively low percentage of apoptosis (1.28%). The administration of siRNA or DTX alone induced only 9.70% and 31.9% apoptosis, whereas the co-administration group induced up to 66.4% apoptosis, which was consistent with the results of CCK-8. These results suggest that the excellent antitumor effect and safety of this biomimetic nanocomplexes may make it a promising delivery system for anticancer drugs.

The downregulation of Bcl-2 gene expression in 4T1 cells was assessed using biomimetic nanocomplexes through Western blot analysis. Figure 5F demonstrates that the application of free Bcl-2 siRNA in 4T1 cells did not result in a significant downregulation of the target protein, potentially due to the sequestration and degradation of free siRNA by lysosomes. However, compared with Free siRNA, E-cLip-DTX / si can effectively reduce the expression of Bcl-2 gene, indicating that the positive charge carried by biomimetic nanocomplexes can not only effectively load Bcl-2 siRNA, but also effectively promote its cell internalization and protect its lysosomal escape into the cytoplasm to exert RNAi effect.

In vivo Antitumor Effects of E-cLip-DTX / Si

We established breast cancer model mice to assess the effects of E-cLip-DTX/si in vivo. Firstly, we prepared DIR-labeled cLip and E-cLip and investigated the tumor enrichment ability of nanoparticles by Alliance Q9 Chemiluminescence Imaging. The results showed that E-cLip-DIR was more enriched at tumor sites than cLip-DIR and free DIR, while the fluorescence of liver sites was weaker (Figure 6A and B), consistent with the results of the in vitro experiments. It was demonstrated that the E-cLip after exosome membrane fusion was able to reduce the clearance in liver sites and increase drug transport to tumor sites.

To gain insight into the therapeutic potential of exosome-based delivery, we investigated their anti-tumor efficacy by injecting different preparations into breast cancer mice (Figure 6C). When the tumor volume is approximately 50–100 cubic millimeters, injections are administered via the tail vein using different preparations, once every three days, for a total of six injections. Mice were euthanized after 18 days of drug treatment, and tumors were excised and photographed and weighed.

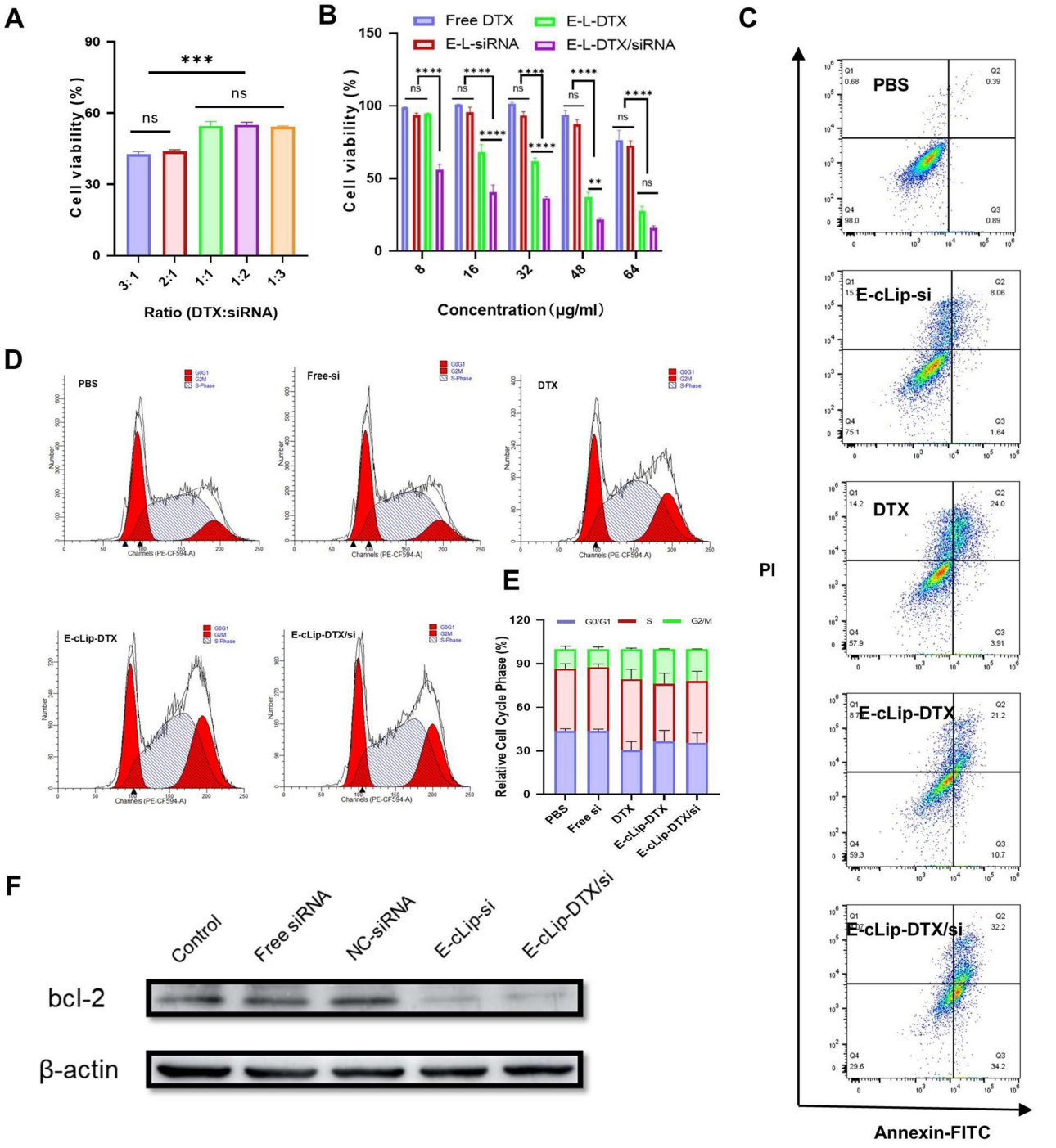

Figure 5 In vitro antitumor effects of the biomimetic nanocomplexes (E-cLip-DTX/si). (**A**) Inhibitory effects of different ratios of DTX and siRNA on 4T1 cells. (**B**) Cell viability of 4T1 cells treated with different formulations. (**C**) Apoptosis of 4T1 cells after treatment with different preparations. (**D**) Cell cycle of 4T1 cells after treatment with different preparations. (**E**) Cell cycle quantification is treated with different preparations. (**F**) Immunoblot analysis of Bcl-2 protein. Data are presented as mean ± standard deviation (n = 3, ****p < 0.0001, ***p < 0.001, **p < 0.01, ns, not significant).

As depicted in Figure 6D, both the DTX and siRNA monotherapy groups demonstrated partial tumor growth inhibition compared to the untreated group (PBS). However, free siRNA exhibited minimal inhibitory effects due to its in vivo instability, consistent with previous findings. Notably, the co-administration group E-cLip-DTX/si displayed the most potent anti-tumor effect, benefiting from reduced phagocytosis by the MPS system and a high tumor accumulation rate. Similar to the tumor volume, the tumor image and tumor weight exhibited the same trend. (Figure 6E and G).

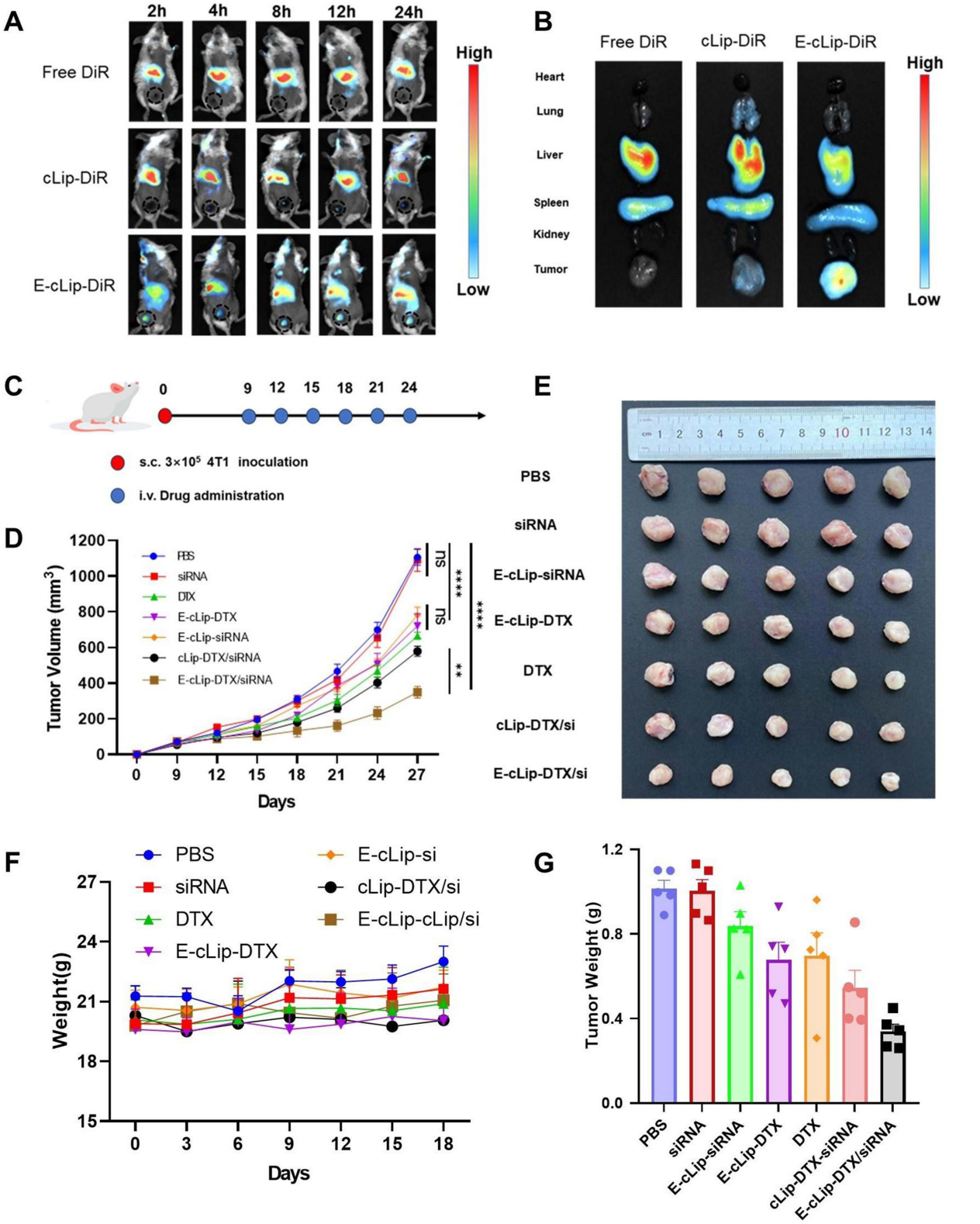

Figure 6 Assessment of in vivo antitumor efficacy of DTX in various formulations. (**A**) Visualization of fluorescence distribution in different nanoparticles using the Alliance Q9 chemiluminescence imaging system at specified intervals, (**B**) followed by tumor removal and examination of fluorescence distribution in major organs after 24 hours. (**C**) Schedule of treatment and analysis. (**D**) Graph illustrating the change in tumor volume. (**E**) Image of excised tumor and (**G**) its weight. (**F**) Monitoring of body weight changes in mice throughout the treatment period. The data is presented as mean ± SD (n = 3, ****p < 0.0001, **p < 0.01, ns, not significant).

https://doi.org/10.2147/IJN.S514375

In addition, there was no significant change in the body weight of the mice throughout the treatment (Figure 6F), and H & E staining of vital organs (Figure 7A) showed that no major organs had organic damage after the combination treatment, which indicated that the drug had good biosafety. Immunohistochemical staining experiments detected the expression of relevant proteins like Ki67 and Bcl-2 in tumor sections. The results indicated that E-cLip-DTX / si significantly decreased Ki67 and Bcl-2 levels compared to control and single drug groups. Furthermore, TUNEL assay showed that E-cLip-DTX / si treatment notably boosted tumor cell apoptosis, as shown by the largest brown stained area (Figure 7B). These findings demonstrate that in E-cLip-DTX / si could accumulate at the tumor site, causing synergistic therapeutic effects and reducing Bcl-2 expression levels. These findings indicate that E-cLip-DTX/si can accumulate at

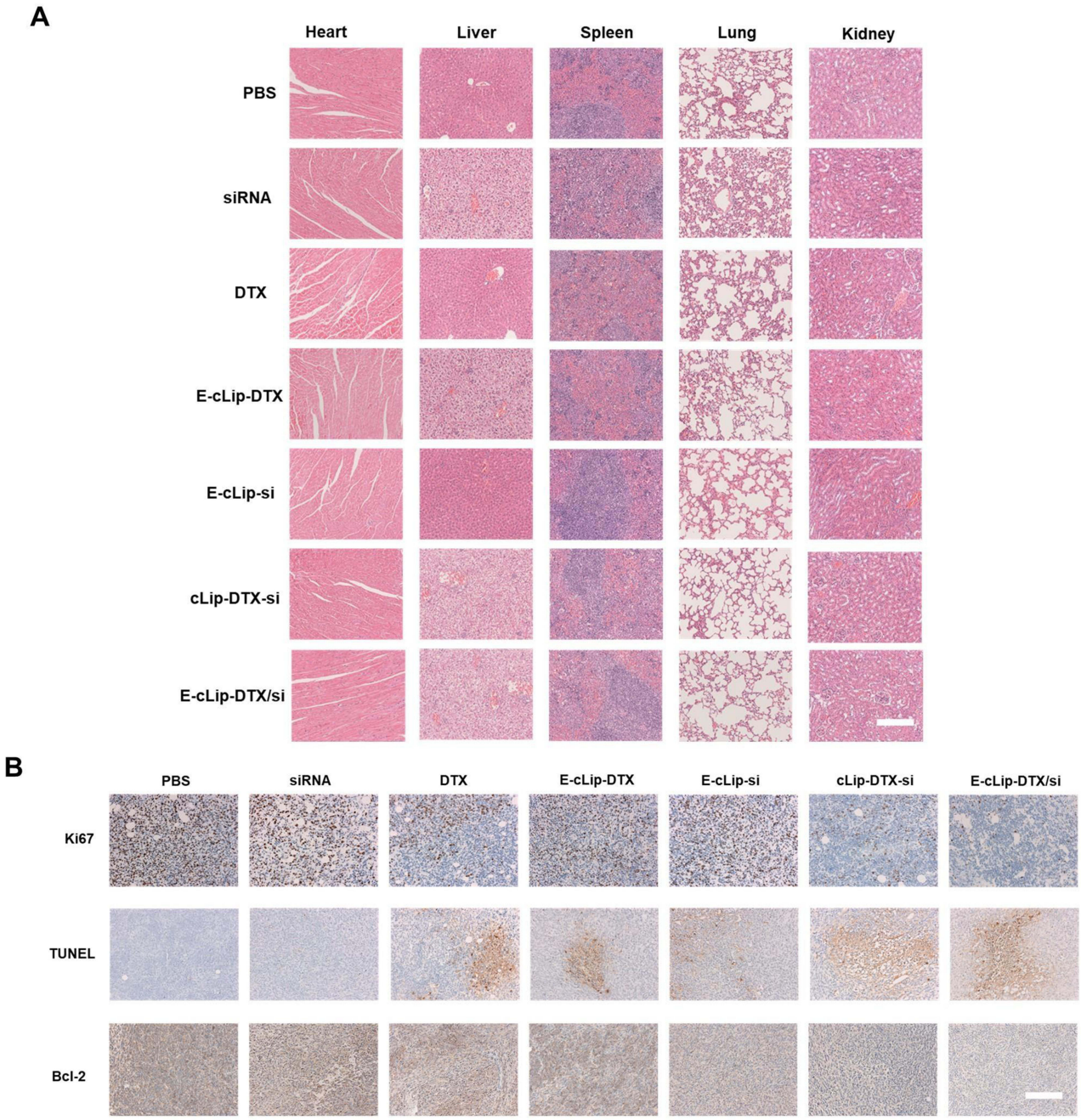

Figure 7 Pathological slides and immunohistochemical analysis. (**A**) Histological section of heart, liver, spleen, lung and kidney organs of BALB/c mice after different treatments. Scale bar: 100 μm. (**B**) TUNEL analysis, Ki67 and Bcl-2 IHC analysis of all post-treatment tumor sections. Scale bar: 100 μm.

tumor sites, reduce the expression level of Bcl-2, effectively promote apoptosis and inhibit the proliferation of tumor cells, and achieve excellent anti-tumor effects.

Discussion

Currently, much attention is being paid to the delivery of drugs for tumor therapy via nanocarriers, which are injected intravenously into the systemic circulation. Nanomedicines are usually passively enriched in tumor tissues through " enhanced permeability and retention effect" (EPR). Specifically, during the formation of solid tumors, the vascular endothelial cells of solid tumors tend to be poorly aligned with gaps, which enhances the permeability of the nanoparticles and allows them to enter the tumor. However, nanomedicines that want to achieve as much enrichment in the tumor region as possible require longer circulating half-life and avoidance of capture by the monocyte phagocytosis system. The biomimetic nanocomplexes in this study achieved longer blood circulation time and reduced MPS capture than ordinary nanoparticles by incorporating macrophage-derived exosomes. Although nanoparticles can be passively targeted to tumor tissues by EPR, there are still limitations to this method. To achieve efficient and precise drug enrichment at the tumor site, EPR alone is not sufficient. To further expand the therapeutic potential of biomimetic nanocomplexes in the clinic, it is necessary for us to further consider targeted modification of nano-delivery platforms for better drug delivery capabilities in the future. Examples include enhancing the active targeting ability-targeting the extracellular matrix,[49] exploiting the chemotaxis function of exosomes themselves,[50] and functionalized modification of the exosome surface. These approaches can significantly enhance the accumulation and penetration efficiency of biomimetic nanocomplexes in tumor tissues, thus achieving more efficient and precise drug delivery. In addition, another important exploration direction for biomimetic nanocomplexes in tumor therapy is to expand diverse combination therapies, such as combined immunotherapy and photodynamic therapy.[51,52] By integrating multiple therapeutic means to achieve synergistic effects, thus significantly enhancing the therapeutic effects and providing patients with more personalized, efficient and safe tumor treatment solutions. This will help promote the development of the field of tumor treatment and improve the quality of survival and prognosis of patients.

It is worth noting that safety has always been emphasized as a part of the clinical application of nanomedicines. Many nanomedicines with translational potential have been terminated due to toxicity issues. Therefore, how to replace the excipients in the formulations with safer and biodegradable biomaterials to reduce the potential toxicity of the formulations is also the focus of our future research.

Conclusion

In summary, we have developed a ROS-responsive biomimetic nanocomplexes that efficiently deliver DTX and Bcl-2 siRNA into the tumor site, overcoming the MPS barrier and extending the blood circulation time of the drug. Our findings demonstrate that the positive charge in the carrier effectively loads siRNA and enables its escape from lysosomal capture to exert its biological function. Additionally, biomimetic nanocomplexes can respond to high levels of ROS in tumor cells, releasing drugs such as DTX to inhibit tumor cell proliferation. Meanwhile, the released DTX also stimulated the cells to further generate ROS, which promoted vector cleavage and further drug release. The experimental results demonstrate that the combination strategy of chemotherapy drugs and RNAi exhibits synergistic anti-tumor effects both in vitro and in vivo. Therefore, biomimetic nanocomplexes hold promise as potential platforms for co-delivering siRNA and chemotherapeutic drugs to enhance the therapeutic efficacy against breast cancer.

Abbreviations

MPS, Mononuclear phagocyte system; cLip, cationic liposomes; Exo, Exosomes; E-cLip-DTX/si, Biomimetic nanocomplexes loaded with Docetaxel and siRNA; EVs, Extracellular vesicles; DTX, Docetaxel; RNAi, RNA interfering; siRNA, Small interfering RNA; NBC, 4-nitrophenyl 4-(4,4,5,5-tetramethyl-1,3,2-dioxaborolan-2-yl) benzyl carbonate; DC-Chol, DC cholesterol; ROS, Reactive oxygen species; MDR, Multidrug resistance; RISC, RNA-induced silencing complex; FT-IR, Fourier transform infrared spectroscopy; ^{1}H NMR, Proton nuclear magnetic resonance spectroscopy; FITC, fluorescein isothiocyanate; FRET, Fluorescent Resonance Energy Transfer; NC-siRNA, Negative Control-siRNA; CLSM,

Confocal laser microscopy; DLS, Dynamic Light Scattering; TEM, Transmission electron microscope; PDI, Polydispersity index; CCK-8, Cell counting kit-8; CI, Combination Index.

Data Sharing Statement

The data that support the findings of this study are available on request from the corresponding author, Jing Xie, upon reasonable request.

Ethics Approval and Consent to Participate

The Institutional Ethics Committee of Chongqing University of Technology approved the animal study protocol.

Supporting Information to Support the Findings Reported in the Paper

Supplementary data to this article can be found.

Funding

This work was supported by Science and Technology Innovation Key R&D Program of Chongqing (No. 2024CCZ096); The Natural Science Foundation Project of CQCSTC (No. cstc2021-jcyj-msxmX0382,); Science and Technology Research Program of Chongqing Municipal Education Commission (Grant No. KJQN202101140); The Graduate Scientific Research and Innovation Foundation of Chongqing, China (No. CYS240721); National Natural Science and Social Science Cultivation Project of Chongqing University of Technology; National Natural Science Foundation of China (22307012); Chongqing Natural Science Foundation Postdoctoral Science Fund Project(CSTB2023NSCQ-BHX0210).

Disclosure

The author(s) report no conflicts of interest in this work.

References

1. Giaquinto AN, Sung H, Miller KD, et al. Breast cancer statistics, 2022. *CA Cancer J Clin*. 2022;72(6):524–541. doi:10.3322/caac.21754
2. Cortes J, Hurvitz SA, Im SA, et al. Trastuzumab deruxtecan versus trastuzumab emtansine in HER2-positive metastatic breast cancer: long-term survival analysis of the DESTINY-Breast03 trial. *Nat Med*. 2024;30:2208–15.
3. Tharp KM, Kersten K, Maller O, et al. Tumor-associated macrophages restrict CD8+ T cell function through collagen deposition and metabolic reprogramming of the breast cancer microenvironment. *Nat Cancer*. 2024;5:1045–62.
4. Chen Z, Xu L, Shi W, et al. Trends of female and male breast cancer incidence at the global, regional, and national levels, 1990-2017. *Breast Cancer Res Treat*. 2020;180(2):481–490. doi:10.1007/s10549-020-05561-1
5. Cannioto RA, Hutson A, Dighe S, et al. Physical activity before, during, and after chemotherapy for high-risk breast cancer: relationships with survival. *J Natl Cancer Inst*. 2021;113(1):54–63. doi:10.1093/jnci/djaa046
6. Mercogliano MF, Bruni S, Mauro FL, Schillaci R. Emerging targeted therapies for HER2-positive breast cancer. *Cancers*. 2023;15:7.
7. Ye F, Dewanjee S, Li Y. Advancements in clinical aspects of targeted therapy and immunotherapy in breast cancer. *mol Cancer*. 2023;22(1):105. doi:10.1186/s12943-023-01805-y
8. Zheng DW, Gao F, Cheng Q, et al. A vaccine-based nanosystem for initiating innate immunity and improving tumor immunotherapy. *Nat Commun*. 2020;11(1):1985. doi:10.1038/s41467-020-15927-0
9. Zhang N, Ping W, Xiang J, et al. Biomimetic single-atom nanozyme for dual starvation-enhanced breast cancer Immunotherapy. *Adv Healthc Mater*. 2024;14:e2401362. doi:10.1002/adhm.202401362
10. Braybrooke J, Bradley R, Gray R. Anthracycline-containing and taxane-containing chemotherapy for early-stage operable breast cancer: a patient-level meta-analysis of 100 000 women from 86 randomised trials. *Lancet*. 2023;401(10384):1277–1292. doi:10.1016/S0140-6736(23)00285-4
11. Gao L, Meng F, Yang Z, et al. Nano-drug delivery system for the treatment of multidrug-resistant breast cancer: current status and future perspectives. *Biomed Pharmacother*. 2024;179:117327. doi:10.1016/j.biopha.2024.117327
12. Anand U, Dey A, Chandel AKS, et al. Cancer chemotherapy and beyond: current status, drug candidates, associated risks and progress in targeted therapeutics. *Genes & Diseases*. 2023;10(4):1367–1401.
13. Fan R, Tao X, Zhai X, et al. Application of aptamer-drug delivery system in the therapy of breast cancer. *Biomed Pharmacother*. 2023;161:114444. doi:10.1016/j.biopha.2023.114444
14. Szakács G, Paterson JK, Ludwig JA, Booth-Genthe C, Gottesman MM. Targeting multidrug resistance in cancer. *Nat Rev Drug Discov*. 2006;5(3):219–234. doi:10.1038/nrd1984
15. Liu Y, Hu Y, Xue J, et al. Advances in immunotherapy for triple-negative breast cancer. *mol Cancer*. 2023;22(1):145. doi:10.1186/s12943-023-01850-7
16. Sandbhor P, Palkar P, Bhat S, John G, Goda JS. Nanomedicine as a multimodal therapeutic paradigm against cancer: on the way forward in advancing precision therapy. *Nanoscale*. 2024;16(13):6330–6364. doi:10.1039/D3NR06131K
17. Gupta A, Andresen JL, Manan RS, Langer R. Nucleic acid delivery for therapeutic applications. *Adv Drug Deliv Rev*. 2021;178:113834. doi:10.1016/j.addr.2021.113834

18. Gondi CS, Rao JS. Concepts in in vivo siRNA delivery for cancer therapy. *J Cell Physiol*. 2009;220(2):285–291. doi:10.1002/jcp.21790
19. Aagaard L, Rossi JJ. RNAi therapeutics: principles, prospects and challenges. *Adv Drug Deliv Rev*. 2007;59(2–3):75–86. doi:10.1016/j.addr.2007.03.005
20. Singh S, Narang AS, Mahato RI. Subcellular fate and off-target effects of siRNA, shRNA, and miRNA. *Pharm Res*. 2011;28(12):2996–3015. doi:10.1007/s11095-011-0608-1
21. Ozpolat B, Sood AK, Lopez-Berestein G. Liposomal siRNA nanocarriers for cancer therapy. *Adv Drug Deliv Rev*. 2014;66:110–116. doi:10.1016/j.addr.2013.12.008
22. Kalluri R, LeBleu VS. The biology, function, and biomedical applications of exosomes. *Science*. 2020;367:6478. doi:10.1126/science.aau6977
23. Meldolesi J. Exosomes and ectosomes in intercellular communication. *Curr Biol*. 2018;28(8):R435–r444. doi:10.1016/j.cub.2018.01.059
24. Tenchov R, Sasso JM, Wang X, Liaw WS, Chen CA, Zhou QA. Exosomes─nature's lipid nanoparticles, a rising star in drug delivery and diagnostics. *ACS Nano*. 2022;16(11):17802–17846. doi:10.1021/acsnano.2c08774
25. Zhang Y, Cai K, Li C, et al. Macrophage-membrane-coated nanoparticles for tumor-targeted chemotherapy. *Nano Lett*. 2018;18(3):1908–1915. doi:10.1021/acs.nanolett.7b05263
26. Das CK, Jena BC, Banerjee I, et al. Exosome as a novel shuttle for delivery of therapeutics across biological barriers. *Mol Pharm*. 2019;16(1):24–40. doi:10.1021/acs.molpharmaceut.8b00901
27. Elliott RO, He M. Unlocking the power of exosomes for crossing biological barriers in drug delivery. *Pharmaceutics*. 2021;13:1. doi:10.3390/pharmaceutics13010122
28. Lu M, Huang Y. Bioinspired exosome-like therapeutics and delivery nanoplatforms. *Biomaterials*. 2020;242:119925. doi:10.1016/j.biomaterials.2020.119925
29. Lu M, Xing H, Xun Z, et al. Functionalized extracellular vesicles as advanced therapeutic nanodelivery systems. *Eur J Pharm Sci*. 2018;121:34–46. doi:10.1016/j.ejps.2018.05.001
30. Bozzuto G, Molinari A. Liposomes as nanomedical devices. *Int J Nanomedicine*. 2015;10:975–999. doi:10.2147/IJN.S68861
31. van der Koog L, Gandek TB, Nagelkerke A. Liposomes and extracellular vesicles as drug delivery systems: a comparison of composition, pharmacokinetics, and functionalization. *Adv Healthc Mater*. 2022;11(5):e2100639. doi:10.1002/adhm.202100639
32. Zylberberg C, Matosevic S. Pharmaceutical liposomal drug delivery: a review of new delivery systems and a look at the regulatory landscape. *Drug Deliv*. 2016;23(9):3319–3329. doi:10.1080/10717544.2016.1177136
33. Liu J, Wu Z, Liu Y, et al. ROS-responsive liposomes as an inhaled drug delivery nanoplatform for idiopathic pulmonary fibrosis treatment via Nrf2 signaling. *J Nanobiotechnology*. 2022;20(1):213. doi:10.1186/s12951-022-01435-4
34. Wang Y, Wang Z, Jia F, et al. CXCR4-guided liposomes regulating hypoxic and immunosuppressive microenvironment for sorafenib-resistant tumor treatment. *Bioact Mater*. 2022;17:147–161. doi:10.1016/j.bioactmat.2022.01.003
35. Kong L, Zhang SM, Chu JH, et al. Tumor microenvironmental responsive liposomes simultaneously encapsulating biological and chemotherapeutic drugs for enhancing antitumor efficacy of NSCLC. *Int J Nanomedicine*. 2020;15:6451–6468. doi:10.2147/IJN.S258906
36. Thakkar S, Sharma D, Kalia K, Tekade RK. Tumor microenvironment targeted nanotherapeutics for cancer therapy and diagnosis: a review. *Acta Biomater*. 2020;101:43–68. doi:10.1016/j.actbio.2019.09.009
37. Tsoi KM, MacParland SA, Ma XZ, et al. Mechanism of hard-nanomaterial clearance by the liver. *Nat Mater*. 2016;15(11):1212–1221. doi:10.1038/nmat4718
38. Inglut CT, Sorrin AJ, Kuruppu T, et al. Immunological and Toxicological Considerations for the Design of Liposomes. *Nanomaterials*. 2020;10:2. doi:10.3390/nano10020190
39. Guo L, Miao Y, Wang Y, et al. Biomimetic macrophage membrane and lipidated peptide hybrid nanovesicles for atherosclerosis therapy. *Adv Funct Mater*. 2022;32(52):2204822. doi:10.1002/adfm.202204822
40. Hu M, Zhang J, Kong L, et al. Immunogenic hybrid nanovesicles of liposomes and tumor-derived nanovesicles for cancer immunochemotherapy. *ACS Nano*. 2021;15(2):3123–3138. doi:10.1021/acsnano.0c09681
41. Chen H, Luo X, Huang Q, et al. Platelet membrane fusion liposome loaded with type I AIE photosensitizer to induce chemoresistance cancer pyroptosis and immunogenic cell death for enhancing cancer immunotherapy. *Chem Eng J*. 2023;476:146276. doi:10.1016/j.cej.2023.146276
42. Li J, Li Y, He Q, Li Y, Li H, Liu L. One-pot native chemical ligation of peptide hydrazides enables total synthesis of modified histones. *Org Biomol Chem*. 2014;12(29):5435–5441. doi:10.1039/C4OB00715H
43. Gao C, Zhang L, Xu M, et al. Pulmonary delivery of liposomes co-loaded with SN38 prodrug and curcumin for the treatment of lung cancer. *Eur J Pharm Biopharm*. 2022;179:156–165. doi:10.1016/j.ejpb.2022.08.021
44. Peng H, Li Y, Ji W, et al. Intranasal Administration of self-oriented nanocarriers based on therapeutic exosomes for synergistic treatment of parkinson's disease. *ACS Nano*. 2022;16(1):869–884. doi:10.1021/acsnano.1c08473
45. Chen M, Miao Y, Qian K, et al. Detachable liposomes combined immunochemotherapy for enhanced triple-negative breast cancer treatment through reprogramming of tumor-associated macrophages. *Nano Lett*. 2021;21(14):6031–6041. doi:10.1021/acs.nanolett.1c01210
46. Tao J, Diao L, Chen F, et al. pH-sensitive nanoparticles codelivering docetaxel and dihydroartemisinin effectively treat breast cancer by enhancing reactive oxidative species-mediated mitochondrial apoptosis. *Mol Pharm*. 2021;18(1):74–86. doi:10.1021/acs.molpharmaceut.0c00432
47. Liu Z, Zhou X, Li Q, Shen Y, Zhou T, Liu X. Macrophage-evading and tumor-specific apoptosis inducing nanoparticles for targeted cancer therapy. *Acta Pharm Sin B*. 2023;13(1):327–343. doi:10.1016/j.apsb.2022.05.010
48. Yuan Q, Han J, Cong W, et al. Docetaxel-loaded solid lipid nanoparticles suppress breast cancer cells growth with reduced myelosuppression toxicity. *Int J Nanomedicine*. 2014;9:4829–4846. doi:10.2147/IJN.S70919
49. De Vita A, Liverani C, Molinaro R, et al. Lysyl oxidase engineered lipid nanovesicles for the treatment of triple negative breast cancer. *Sci Rep*. 2021;11(1):5107. doi:10.1038/s41598-021-84492-3
50. Molinaro R, Martinez JO, Zinger A, et al. Leukocyte-mimicking nanovesicles for effective doxorubicin delivery to treat breast cancer and melanoma. *Biomater Sci*. 2020;8(1):333–341. doi:10.1039/C9BM01766F
51. Ning S, Zhang T, Lyu M, et al. A type I AIE photosensitiser-loaded biomimetic nanosystem allowing precise depletion of cancer stem cells and prevention of cancer recurrence after radiotherapy. *Biomaterials*. 2023;295:122034. doi:10.1016/j.biomaterials.2023.122034
52. Ning S, Lyu M, Zhu D, et al. Type-I AIE photosensitizer loaded biomimetic system boosting cuproptosis to inhibit breast cancer metastasis and rechallenge. *ACS Nano*. 2023;17(11):10206–10217. doi:10.1021/acsnano.3c00326